Nanocrystalline TiO2 micropillar arrays grafted on conductive glass supports: Microscopic and spectroscopic studies

Thin Solid Films

Volume 590, 1 September 2015, Pages 200–206
doi:10.1016/j.tsf.2015.07.058

Thin Solid Films (Elsevier)

Volume 590, 1 September 2015, Pages 200–206

doi:10.1016/j.tsf.2015.07.058

Nanocrystalline TiO_2 micropillar arrays grafted on conductive glass supports: microscopic and spectroscopic studies

Federico Cesano*, Giovanni Agostini, Domenica Scarano

Department of Chemistry, NIS (Nanostructured Interfaces and Surfaces) Interdepartmental Centre, University of Torino, Via P. Giuria, 7, 10125 Torino Italy

Abstract. Vertically oriented TiO_2 micropillar arrays were obtained on Fluorine-doped Tin Oxide (FTO) conductive glasses by adopting a facile and cost-effective method. The process consists in the spray-coating with a polymer film containing an organo-metallic precursor (Ti isopropoxyde), followed by scratching the film surface by means of a sandpaper and an oxidative treatment. The role played by the scratching step in the formation of vertically oriented TiO_2 micropillars, as well as the nanostructured scaffold nature consequent upon the oxidation, will be highlighted. The morphology, structure and optical properties of samples, were investigated by combining electron and atomic force microscopies with X-ray diffraction and UV–vis spectroscopy. Due to the robust texture of highly crystalline and cemented anatase and rutile nanoparticles and to the porous nature of TiO_2 pillars covering FTO glasses, this system may find application in energy, photochemistry and photodegradation fields.

1. Introduction

In the past years, the interest of 1D, 2D and 3D metal oxides and semiconductors has been increased by the fact that these nanostructures have their peculiar electronic and optical properties shape/structure dependent [1–6]. TiO_2-based nanosystems have paved the way for the enhancement of properties (i.e. photocatalytic properties, photostability, high photoconversion efficiency and chemical inertness), which find applications in a wide variety of fields, including dye sensitized solar cells, photocatalysis, water splitting, gas sensors, photodegradation of organic pollutants and optoelectronic devices [7]. Although all these application fields represent clean and sustainable solutions, they need still some improvements for a wider diffusion.

As far as dye photodegradation is concerned, the fabrication of robust nanoengineered TiO_2 coating plays a crucial role. In fact, the high photocatalytic activity, induced by isolated nanoparticles, is not the exclusive requisite for practical applications. The separation of TiO_2 material from the solution after irradiation is necessary as well as the presence of a hierarchical porosity, providing a fast accessibility and a facile fluid transport may be mandatory for an efficient use of the material in the industrial applications [8]. As far as dye-sensitized solar cells (DSSCs) are concerned, an overall light-to-electricity conversion efficiency of ~12% has been obtained [9,10]. The overall process is complex, mainly ruled by many factors, including the light-harvesting efficiency, type and stability of the adsorbed-dye (i.e. Ru-based dyes), photoanode properties (i.e. crystallinity, the porosity of TiO_2 film and its thickness), charge-transport efficiency, photocurrent density, conductivity and optical transparency of the glass electrodes and interface properties (i.e. TiO_2/adsorbed dye, TiO_2 grain boundaries, TiO_2 film/electrode interfaces) [7,11]. Some of the strategies in "bridging the gap" between theoretical and experimental performances of DSSCs are pursued, such as the doping of the TiO_2 the nano-engineering of the surface [12,13] and the addition of quantum dots (e.g. CdS/CdSe) [14]. Furthermore, the incorporation of high-surface-area carbon nanotubes or amorphous carbon could be beneficial for the exciton dissociation and charge-carrier transport, thus improving the power conversion efficiency [15] or the photocatalytic activity of TiO_2/C composites [16]. On the other hand, the electronic properties and the efficiency of the light harvesting process can be tuned, by tailoring phase composition, crystallinity, surface roughness, porosity, shape and crystal size of TiO_2-based materials [2,11]. By playing with several methods of preparation (sol–gel, chemical etching, hydrothermal, spray-pyrolysis, chemical and physical vapor deposition techniques) [1], many morphologies and structures can be obtained, such as nanotubes [17] and nanowires (1D) [18], nanoplatelets and nanosheets (2D) [19], spheres [8] and crystals exposing peculiar facets [20], and fibers coated by TiO_2 [21]. However, it is believed that the one dimensional nanostructures are the most attractive candidates for solar energy conversion because of

* Corresponding author. federico.cesano@unito.it
E-mail addresses: (F. Cesano),

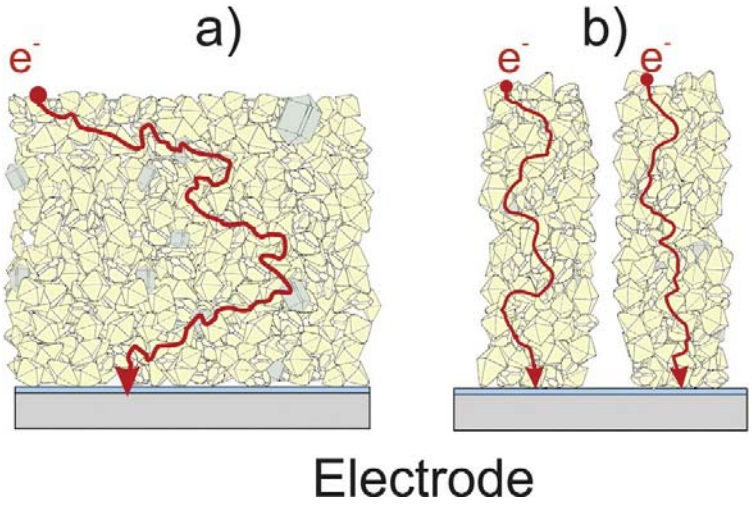

Scheme 1. Schematic representations of the different paths of electrons moving through: a) a polycrystalline film and b) nanostructured TiO_2 pillar arrays.

their direct electrical pathway, which causes a faster charge transport to the electrode, thus greatly reducing recombinations effects and then improving the performance of the optoelectronic devices (Scheme 1). To this purpose, vertically oriented arrays of nanotubes, rods, strips, cones and pillars made of anatase [22–29], rutile [9,30–32] and by mixed anatase-rutile nanostructures [33,34], have been fabricated.

In this work, quasi-regular arrays of vertically oriented micropillars, constituted by assembled TiO_2 nanocrystals on conductive Fluorine-doped Tin Oxide (FTO) coated glass and obtained via a simple preparation method, have been carefully investigated by several microscopy techniques. The preparation method can be summarized, as follows: i) deposition of a polymer film containing a TiO_2 precursor on a conductive FTO-coated glass, ii) scratching of the surface, iii) thermal oxidation of the polymer film, causing the conversion of the Ti organo-metallic compounds to TiO_2.

2. Experimental section

Materials and preparation methods

All reagents were of analytical grade and used without further purification. Fluorine-doped tin oxide coated sodalime glasses (TCO 30-8, Solaronix S.A. — Aubonne, Switzerland, 3 mm thick, resistivity ~7.9 Ω/sq) were used as supports. FTO-coated glasses, cleaned with acetone in an ultrasonication bath, were dipped in a 40 mM aqueous solution of $TiCl_4$ at 343 K for 30 min and washed with ethanol. A polymer film, obtained from a solution of Ti isopropoxyde (TIP) and furfuryl alcohol (FA) (17 wt.% of TIP), was deposited on the glass support by spray-deposition technique. A lab-scale spray dryer was used by means of air as a spray gas (gas flow of 3 L/min for 1.5 s. with a nozzle tip diameter of 0.7 mm) and by placing supports of 2.5 × 2.5 cm at a distance of 10 cm at room temperature. The deposition area has been estimated to be larger than FTO-coated supports. The TIP and FA quantities were selected on the basis of a previous work, in which high-surface-area TiO_2 micropillars were obtained as a bulk material [35]. The polymerization, which is highly exothermic, was controlled by keeping the temperature of the materials at 373 K for 180 min and then by rising up to 473 K (heating rate 2 K/min), as obtained by preliminary differential scanning calorimetry (DSC) analysis (Data not shown for the sake of brevity). A first sample was thermally treated as obtained, while a second sample was scratched by a sandpaper (P1200 grade), along two quasi-perpendicular directions on the polymer surface. The scratching of the sample surface was performed by hands at a labscale with no external control of pressure/time. Three different identical samples were obtained for testing the process reproducibility. Thermal treatment/oxidation steps were performed in N_2/air gas mixture (200 + 40 ml/min) for 20 h at 773 K with a heating rate of 5 K/min.

Characterization techniques

Morphology, composition and structure of the materials have been investigated by means of: i) scanning electron microscopy (SEM; Zeiss Evo50) operating at 20 kV and equipped with an energy dispersive X-ray detector (EDAX); ii) atomic force microscopy (Nanosurf EasyScan2) equipped with a 10 μm high-resolution scan-head operating in contact-mode, located on a high-performance anti-vibration platform and acoustically shielded by means of an insulated enclosure; iii) transmission electron microscopy (TEM; JEOL 3010-UHR) operating at 300 kV and equipped with a 2 k × 2 k pixels Gatan US1000 CCD camera. Reciprocal lattices and simulated electron patterns to obtain crystal orientation were simulated by means of CaRIne Crystallography 3.1 software package.

To minimize effects of the substrate, films have been estimated by using a grazing incidence X-ray diffraction (GIXRD) technique (fixed incident beam of $\alpha = 1.8°$) in a PANalytical X'Pert PRO diffractometer working with a Ni-filtered $Cu_{k\alpha}$ radiation. The mean crystallite size was calculated from XRD measurements by Scherrer's equation: $L = K\lambda/\beta \cos\theta$, where λ is the X-ray wavelength, β is the full width at half maximum (FWHM) of the diffraction line corrected by the instrumental broadening, θ is the diffraction angle, and K is a constant, which has been assumed to be 0.9 for TiO_2 and SnO_2. Simulated XRD patterns in restricted 2θ regions were fitted by a Pseudo-Voigt function.

Differential scanning calorimetry (DSC) analyses were performed at different increasing rate (2–5 K/min) by means of a Q200 TA Instruments equipment.

Conductive-AFM (C-AFM) analyses were performed by applying a moderate and negative bias (−1.5 V) on the tip (tip radius ≥ 25 nm, 5 nm Chromium and 25 nm Platinum coated on both sides). In addition, a 500 kΩ resistor was connected in series to reduce the current passing through the tip probe.

Electrical measurements on conductive glass were obtained by using a four point probe resistivity measurements (Jandel four-point-probe-head connected with a Keithley 2420 source meter/analyzer).

3. Results and discussion

Morphology, structure and electrical properties of the FTO electrodes

The morphology and the structure of the FTO conductive glass are shown in Fig. 1. The low resolution SEM image shows an incidentally damaged region of the conductive layer (Fig. 1a).

In this image, dark and bright regions are associated with the different local surface charging properties, which are induced by the acceleration potential [6,36,37]. Higher resolution SEM and AFM images of the FTO-coated glass are reported in Fig. 1b and c, respectively, where nanocrystals (~30–300 nm in size), having irregular habit and exposing rough surfaces, are shown. The local electrical properties (or map of current) of the AFM imaged region in Fig. 1c, are shown in Fig. 1d. The presence of bright and irregular features (evidenced by arrows in Fig. 1d) can be observed. These regions, corresponding to more conductive areas, are located in a more extended dark region, insulating in character. Notice that the higher conductive areas are associated with the same terminations of the particles shown in Fig. 1c, in particular with crystal edges, inverse-steps "coupled" with edges and corners, typical of polycrystalline/granular surfaces [38]. It is noteworthy that, as the conductive tip is working in contact mode, the extent of contacts between tip and surface, together with the nature of the applied force can affect the shape and the dimensions of the conductive regions. However, we can reasonably state that no significant variations were observed within the extent of the used potentials or setpoint loadings.

The conductive film is constituted primarily by Sn and O atoms (Fig. 1e). The XRD pattern of the FTO conductive glass film, as obtained at glacing angle, shows several narrow peaks (Fig. 1f). Among all, those at $\theta \cong 26.4°$, 33.6°, 37.6°, 51.4° are associated to (110), (101), (200), (211) XRD planes of the tetragonal SnO_2 (Cassiterite, PDF card n. #41-1445). As the XRD peak broadening depends on the coherent scattering domains, it is possible to determine the sizes of the SnO_2 crystals by applying the Sherrer's equation to the (110) XRD diffraction planes (Inset of Fig. 1f). A mean value of ~40 nm is obtained, which corresponds to ≈ 119 layers, by considering an interlayer distance of 3.35 Å.

Morphology, structure and optical properties of the TiO_2 polymer precursor and of the TiO_2-coated FTO glasses

Thin polymer films (10–20 μm in thickness), which were obtained from the polymerization of the spray-deposited titanium isoproxyde (TIP) and furfuryl alcohol (FA) liquid solution on FTO-coated glasses, are shown in Fig. 2.

In the past, the method has been effectively used, to obtain high-surface-area mesoporous carbons [39], as well as nanostructured oxides (SnO_2 [33], TiO_2 [35] and ZnO [40]) by starting from an oxide precursor acting as a Lewis acid catalyst to promote the polymerization of furfuryl alcohol. In Fig. 2 the polymer film is AFM/SEM imaged before (Fig. 2a–c) and SEM imaged after thermal treatment in air at 773 K (Fig. 2d–f). From AFM images it comes that, before the thermal treatment, the polymer film is highly homogeneous and regularly adhering to the substrate, with a roughness lower than ~1 nm (see AFM height-profile of a selected line in Fig. 2c). Conversely, after thermal treatment in air at 773 K, the film results to be highly damaged and only partially adhering to the FTO-coated glass (Fig. 2d–f). Notice that, it is made by irregularly fragmented domains over 20 μm in size and about 20 μm in thickness (insert in Fig. 2f), which appear markedly different from the "thick" (i.e. bulk) nanostructured TiO_2 material reported in [35], although prepared by adopting similar experimental conditions.

In order to prevent the irregular cracking of the film and to obtain a more regular morphology, a different approach was adopted. In more detail, before the oxidation treatment, the polymer film covering the FTO coated glass was scratched by a sandpaper. The scratched polymer surface is AFM imaged in Fig. 3a–c.

From these images (Fig. 3a and c), a periodic surface made of grooves about 2.5–3 μm spaced, is evidenced, as testified by the fast-Fourier-transform (FFT) shown in the inset of Fig. 3a. The height profiles along two perpendicular directions (Fig. 3b) are confirming the regular patterned surface.

It will be shown that such grooves play a role in the generation of a more regular surface during the oxidation step (vide infra). The morphology, the structure and the chemical composition of the oxidized film on the FTO-coated glass, are reported in Fig. 4a–f.

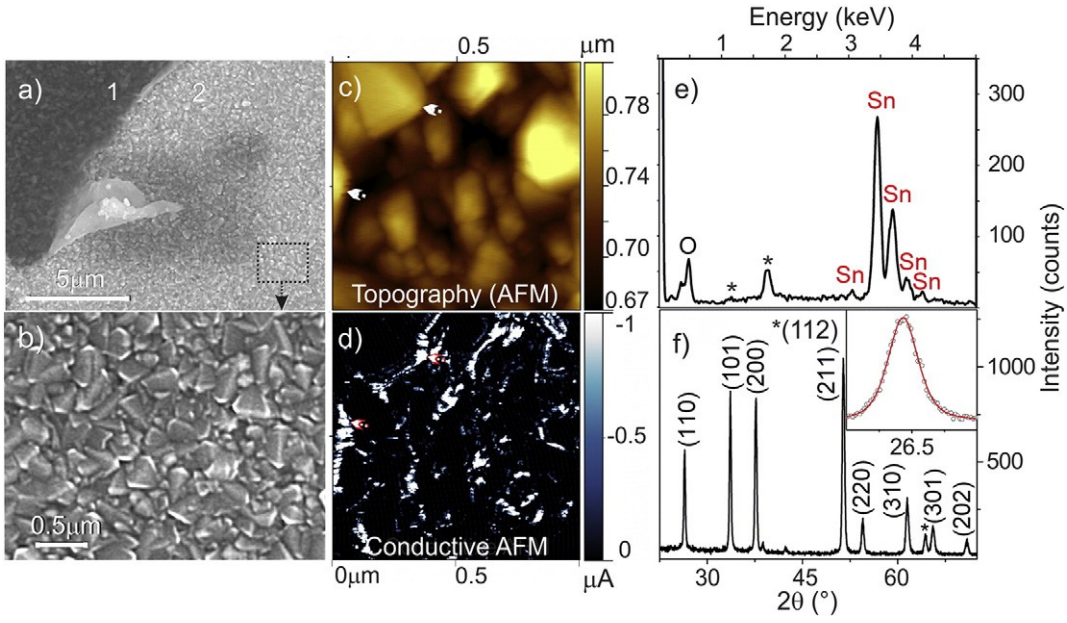

Fig. 1. Images of the FTO glass support: a) low resolution SEM: regions evidenced by 1 and 2 (dark and bright contrast, respectively) refer to incidentally damaged and to FTO-coated conductive areas; b) enlarged view of a selected area in a); c) contact mode AFM topography; d) conductive-AFM (c-AFM) of the same region shown in c); e) EDAX elemental analysis (asterisks refer to the underlying phase) and f) grazing angle XRD pattern of the FTO film on the glass. Arrows in c) and d) refer to two high conductive regions of the polycrystalline film, while the simulated XRD pattern by a Pseudo-Voigt function in the $2\theta \cong 26–27°$ range, is reported in the inset of f).

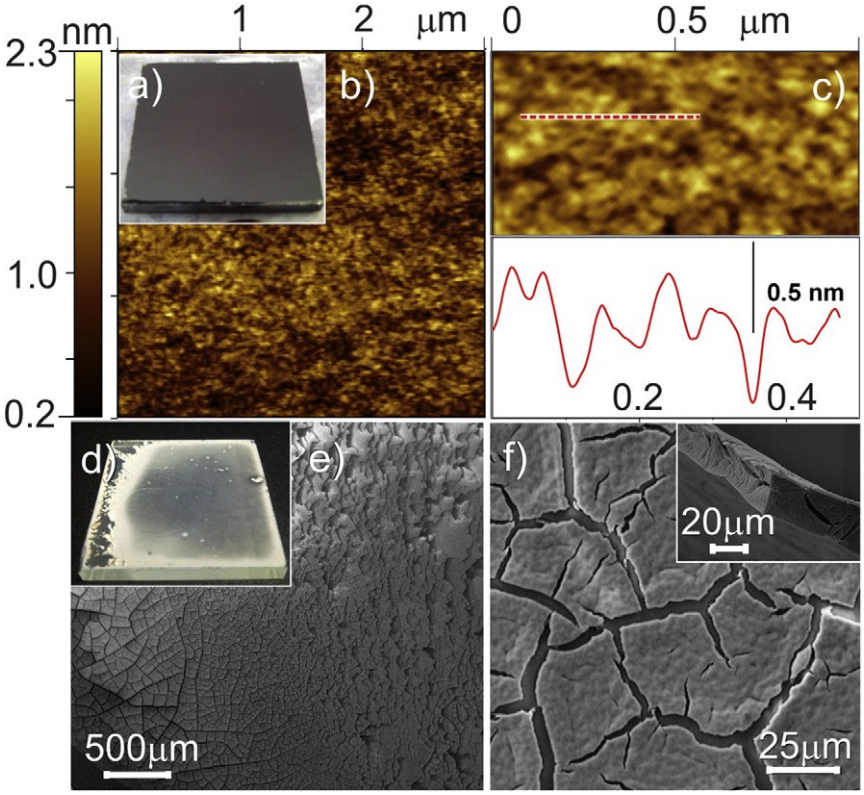

Fig. 2. (a, b, c) Images of the polymer film covering the FTO-coated glass, before thermal treatment in air at 500 °C: a) picture; b) and c) AFM images at different level of magnification: on the bottom of c) the AFM height-profile of the selected line is shown; (d, e, f) images of the polymer film covering the FTO-coated glass, after thermal treatment in air at 500 °C: d) picture; e) and f) SEM images at different level of magnification. Lateral view of the polymer film (inset in panel 2f).

SEM images (top- and lateral-views, in Fig. 4b and c, respectively) evidence that the obtained film is macroporous, being constituted by pillared microstructures, which are quasi-regularly spaced. Moreover the SEM image of a selected-area (Fig. 4d) shows that the porous film, about 5–7 μm in thickness, is formed of a regular carpet of short pillars about 5–10 μm wide. The chemical composition, taken on the top of a pillar, is mainly dominated by O and Ti, as comes from EDAX analysis (Fig. 4e). In order to investigate the crystallinity of the film, the XRD diffraction pattern has been obtained at a grazing angle (Fig. 4f). The pattern shows several narrow XRD peaks. Among all, those at $\theta \sim 25.2°$, 37.8°, 48.0° and at 27.5°, 36.1°, 41.2°, 54.3° are related to (101), (004), (200) and to (110), (101), (111), (211) XRD diffraction planes of anatase (TiO_2, PDF card n. #21-1272) and of rutile (TiO_2, PDF card n. #21-1276), respectively. The 88/12 anatase/rutile phase ratio was obtained from the reference intensity ratio (RIR) values. By applying the Scherrer's equation to the (101) anatase and the (110) rutile XRD diffraction peaks, (inset of Fig. 4f) mean values of about 13 nm and about 14 nm are obtained, respectively. The high crystallinity of the TiO_2 nanocrystals is also testified by the diffraction profile obtained in the $36 \div 39° \ 2\theta$ range, where distinct peaks, associated to (101) and (103), (004), (112) diffraction planes of rutile and anatase, are shown [8].

More details on the nanostructured TiO_2 film come from high-resolution SEM and TEM images taken on a portion of a TiO_2 micropillar

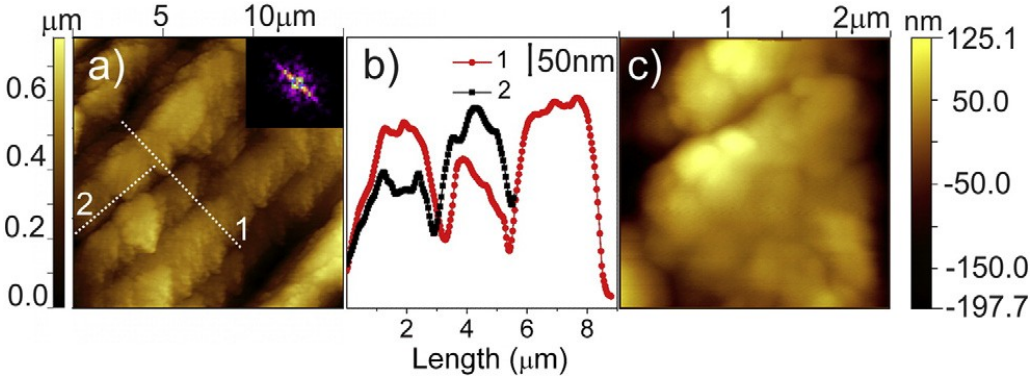

Fig. 3. a) AFM image of the TIP/FA film on the FTO glass after surface scratching: in the inset of a) the fast Fourier transform (FTT) is reported; b) height profiles along the two perpendicular directions shown in a); c) AFM enlarged view of a selected region in a).

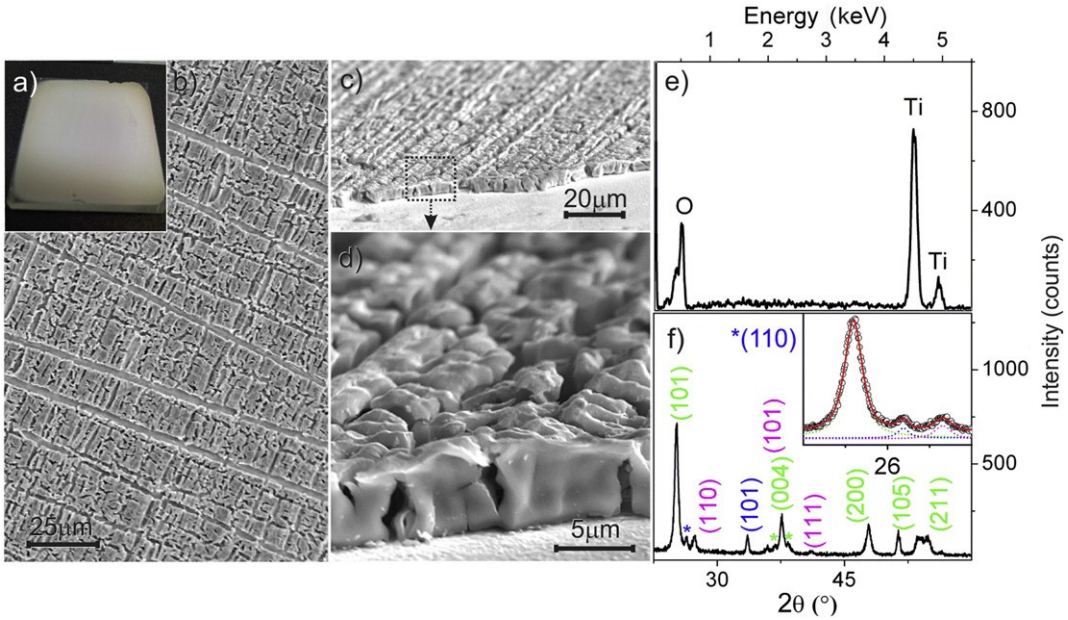

Fig. 4. Images of the scratched TIP/FA film oxidized at 500 °C for 20 h: a) picture; b) on top SEM image; c) lateral-view SEM image; d) enlarged view of a selected-area in c); e) EDAX elemental analysis; f) grazing angle XRD pattern of the columnar TiO_2 anchored to the FTO-coated glass. Colors refer to the different phases: anatase (green), rutile (magenta), SnO_2 (blue). In the inset of f) the simulated XRD pattern in the $2\theta \cong 24–28°$ range is reported.

(Fig. 5a–c). In these images, the presence of cemented nanocrystals (Fig. 5a–b) forming a robust and porous scaffold can be highlighted. The porous nature of the TiO_2 micropillar comes from the TEM image shown in Fig. 5c.

Two selected regions are high-resolution TEM imaged in Fig. 6. The crystalline nature of the TiO_2 single nanocrystals about 5–15 nm in size, is testified by the presence of well-defined interference fringes 0.34 nm and 0.32 nm spaced (Fig. 6a and d, respectively), which correspond to the anatase (101) and rutile (110) crystalline planes, respectively. From the FFT images of the selected regions of Fig. 6a, c (Fig. 6b, e) and from the corresponding simulated electron diffraction patterns (Fig. 6c, f) of the two selected nanocrystals, the anatase [1,1,1] and the rutile [0,0,1] zone-axis directions are obtained, respectively.

The UV–vis diffuse reflectance spectrum of the TiO_2-micropillar arrays in the 350–450 nm range is shown in Fig. 7. Spectra of the nanocrystalline anatase and rutile powders, used as reference materials, are reported in the same figure. From this, the absorption edge of the TiO_2 pillar film is red-shifted, as compared to that of anatase nanocrystals used as a reference. This fact is in agreement with the ascertained presence of rutile nanocrystals, whose absorption edge is occurring at lower energy than that of the "pure" anatase. Although the reason of lowering the TiO_2 bandgap in anatase/rutile mixed-phase is still a debated issue and goes beyond the scope of this work, some considerations can be drawn. Stimulated by the high photocatalitic activity of mixed-phase anatase/rutile TiO_2, a band alignment, presumably caused by interfacial regions/junctions, has been proposed in accordance with experimental evidences [41]. This band alignment would favor the transfer of photogenerated electrons from anatase to rutile and of the holes from rutile to anatase. The nanoengineering of the TiO_2 phase-junctions would increase performances of photocatalytic processes, as well as those of photovoltaic systems [42,43].

4. Conclusions

An alternative, simple, rapid and cost-effective method to produce porous TiO_2 films is reported. Thin polymer films obtained from a TiO_2 precursor (Ti isopropoxyde), working as a Lewis acid catalyst and a polymer precursor (furfuryl alcohol), were deposited

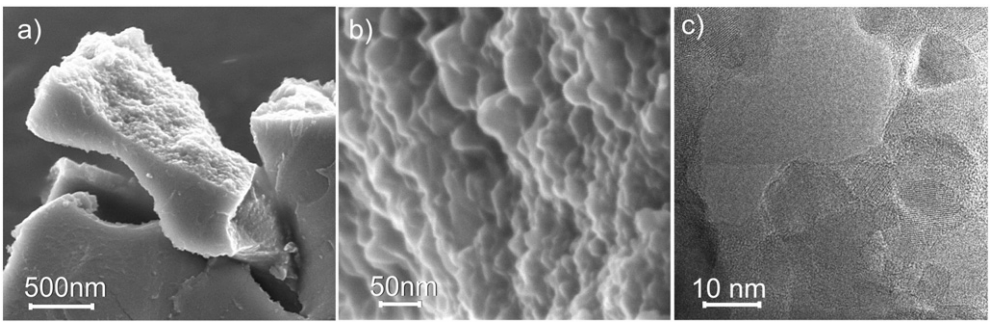

Fig. 5. Images of the internal portions of a TiO_2 micropillar: a) and b) SEM images at different level of magnification and c) TEM image of a TiO_2 micropillar illustrating a mesopore of 10–30 nm, surrounded by well cemented crystalline nanoparticles.

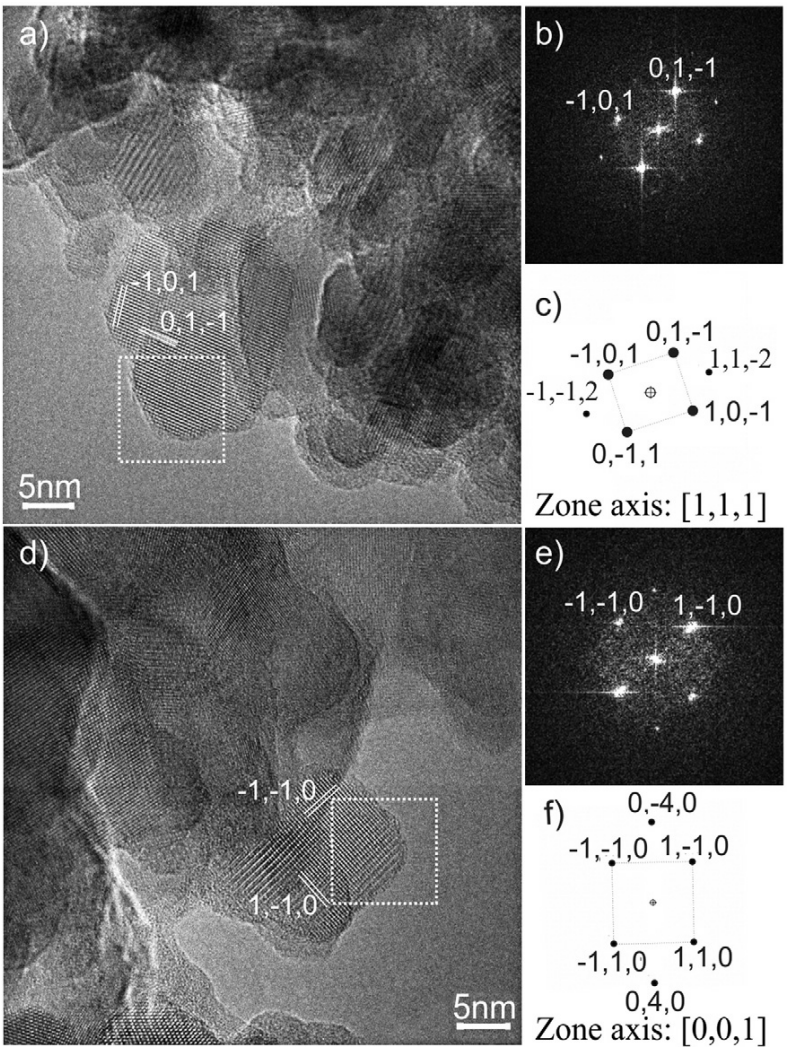

Fig. 6. a) and d) high-resolution TEM images of two selected regions of the TiO_2 micropillars; b) and e) fast-Fourier-transform (FFT) images of the selected nanocrystals in a) and d); c) and f) the corresponding simulated electron diffraction patterns along the [1,1,1] (anatase) and the [0,0,1] (rutile) zone axis directions, respectively.

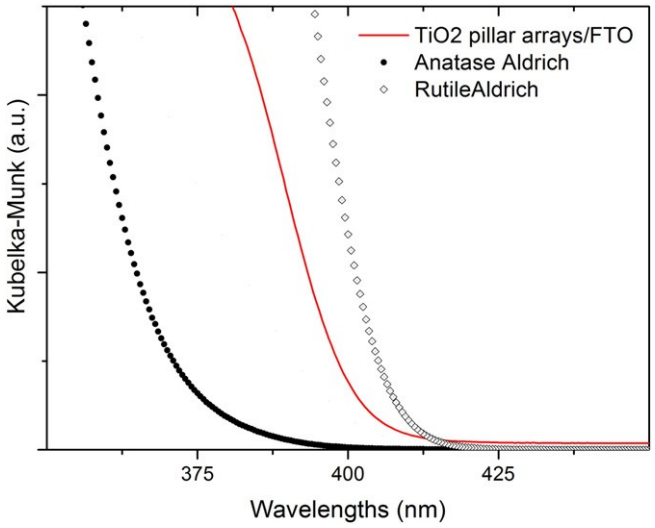

Fig. 7. Diffuse reflectance spectrum of the TiO_2 pillar arrays on FTO-coated glass in the 350–450 nm range, as compared to the reference materials: anatase (●) and rutile (◊) nanoparticles.

on the surface of FTO-conductive glasses by spray-coating technique. Depending on the preparation steps, a film made by quasi-regular arrays of nanostructured TiO_2 micropillars can be obtained. In fact, after thermal oxidation of the polymer film scratched with a sandpaper, vertically oriented TiO_2 micropillar arrays are obtained. The porous nature and the robust texture of the TiO_2 micropillars result from a nanostructured scaffold composed of anatase and rutile nanoparticles, which are highly crystalline and cemented together. The vertical orientation of micropillars, their good adhesion to the conductive glass, and the previously discussed porous nature of the robust TiO_2 scaffold may find application in the energy, photochemistry and photodegradation fields.

This method can be attractive to tailor surfaces with nanostructures, but further optimizations with respect to the desired microstructure are necessary, for example the film thickness, porosity in the micropillar arrays.

Acknowledgments

This work has been partially supported by MIUR (Ministero dell'Istruzione, dell'Università e della Ricerca).

References

[1] X. Chen, S.S. Mao, Titanium dioxide nanomaterials: synthesis, properties, modifications, and applications, Chem. Rev. 107 (2007) 2891.
[2] A. Kubacka, M. Fernandez-García, G. Colon, Advanced nanoarchitectures for solar photocatalytic applications, Chem. Rev. 112 (2012) 1555.
[3] S. Cravanzola, L. Muscuso, F. Cesano, G. Agostini, A. Damin, D. Scarano, A. Zecchina, MoS_2 nanoparticles decorating titanate-nanotube surfaces: combined microscopy, spectroscopy, and catalytic studies, Langmuir 31 (2015) 5469.
[4] L. Muscuso, S. Cravanzola, F. Cesano, D. Scarano, A. Zecchina, Optical, vibrational and structural properties of MoS_2 nanoparticles obtained by exfoliation and fragmenta- tion via ultrasound cavitation in isopropyl alcohol, J. Phys. Chem. C 119 (2015) 3791.
[5] J. Tao, T. Luttrell, M. Batzill, A two-dimensional phase of TiO_2 with a reduced bandgap, Nat. Chem. 113 (2011) 296.
[6] G. Haznedar, S. Cravanzola, M. Zanetti, D. Scarano, A. Zecchina, F. Cesano, Graphite nanoplatelets and carbon nanotubes based polyethylene composites: electrical conductivity and morphology, Mater. Chem. Phys. 143 (2013) 47.
[7] O. Carp, C. Huisman, A. Reller, Photoinduced reactivity of titanium dioxide, Prog. Solid State Chem. 32 (Issue 1-2) (2004) 33.
[8] F. Cesano, D. Pellerej, D. Scarano, G. Ricchiardi, A. Zecchina, Radially organized pillars in TiO_2 and in TiO_2/C microspheres: synthesis, characterization and photocatalytic tests, J. Photochem. Photobiol. A Chem. 242 (2012) 51.
[9] H.-E. Wang, Z. Chen, Y.H. Leung, C. Luan, C. Liu, Y. Tang, C. Yan, W. Zhang, J.A. Zapien, I. Bello, S.-T. Lee, Hydrothermal synthesis of ordered single-crystalline rutile TiO_2 nanorod arrays on different substrates, Appl. Phys. Lett. 96 (2010) 263104.
[10] F. Gao, Y. Wang, D. Shi, J. Zhang, M. Wang, X. Jing, R. Humphry-Baker, P. Wang, S.M. Zakeeruddin, M. Gratzel, Enhance the optical absorptivity of nanocrystalline TiO_2 film with high molar extinction coefficient ruthenium sensitizers for high perfor- mance dye-sensitized solar cells, J. Am. Chem. Soc. 130 (2008) 10720.
[11] T.W. Hamann, R.A. Jensen, A.B.F. Martinson, H.V. Ryswyk, J.T. Hupp, Advancing beyond current generation dye-sensitized solar cells, Energy Environ. Sci. 1 (2008) 66.
[12] X. Lu, X. Mou, J. Wu, D. Zhang, L. Zhang, F. Huang, F. Xu, S. Huang, Improved- performance dye-sensitized solar cells using Nb-doped TiO_2 electrodes: efficient electron injection and transfer, Adv. Funct. Mater. 20 (2010) 509.
[13] M.J. Uddin, F. Cesano, S. Bertarione, F. Bonino, S. Bordiga, D. Scarano, A. Zecchina, Tailoring the activity of Ti-based photocatalysts by playing with surface morphology and silver doping, J. Photochem. Photobiol. A Chem. 196 (2008) 165.
[14] M.J. Uddin, D.E. Daramola, E. Velasquez, J. Yan, E. Hammel, F. Cesano, O.I. Okoli, A high efficiency 3D photovoltaic micro-wire with carbon nanotubes (CNT)-quantum dot hybrid interface, Phys. Status Solidi (RRL) 8 (2014) 898.
[15] J. Yan, M.J. Uddin, T.J. Dickens, O.I. Okoli, Carbon nanotubes (CNTs) enrich the solar cells, Sol. Energy 96 (2013) 239.
[16] G. Zhang, F. Teng, C. Zhao, L. Chen, P. Zhang, Y. Wang, C. Gong, Z. Zhang, E. Xie, Enhanced photocatalytic activity of TiO_2/carbon@TiO_2 core–shell nanocomposite prepared by two-step hydrothermal method, Appl. Surf. Sci. 311 (2014) 384.
[17] F. Cesano, S. Bertarione, M.J. Uddin, G. Agostini, D. Scarano, A. Zecchina, Designing TiO_2 based nanostructures by control of surface morphology of pure and silver loaded titanate nanotubes, J. Phys. Chem. C 114 (2010) 169.
[18] G.K. Mor, O.K. Varghese, M. Paulose, C.A. Grimes, Transparent highly ordered TiO_2 nanotube arrays via anodization of titanium thin films, Adv. Funct. Mater. 15 (2005) 1291.
[19] N.C. Raut, T. Mathews, K. Panda, B. Sundaravel, S. Dash, A.K. Tyagi, Enhancement of electron field emission properties of $TiO_{2(2-x)}$ nanoplatelets by N-doping, RCS Adv. 2 (2012) 812.
[20] H.G. Yang, C.H. Sun, S.Z. Qiao, J. Zou, G. Liu, S.C. Smith, H.M. Cheng, G.Q. Lu, Anatase TiO_2 single crystals with a large percentage of reactive facets, Nature 453 (2008) 638.
[21] L. Chen, S. Yang, E. Mäder, P.-C. Ma, Controlled synthesis of hierarchical TiO_2 nanoparticles on glass fibres and their photocatalytic performance, Dalton Trans. 43 (2014) 12743.
[22] C.K. Lim, H. Huang, C.L. Chow, P.Y. Tan, X. Chen, M.S. Tse, O.K. Tan, Enhanced charge transport properties of dye-sensitized solar cells using TiNxOy nanostructure composite photoanode, J. Phys. Chem. C 116 (2012) 19659–19664.
[23] X. Dong, J. Tao, Y. Li, H. Zhu, Oriented single crystalline TiO_2 nano-pillar arrays directly grown on titanium substrate in tetramethylammonium hydroxide solution, Appl. Surf. Sci. 256 (2010) 2532.
[24] Y.-K. Lai, Y.-X. Tang, J.-Y. Huang, F. Pan, Z. Chen, K.-Q. Zhang, H. Fuchs, L.-F. Chi, Bioinspired TiO_2 nanostructure films with special wettability and adhesion for droplets manipulation and patterning, Sci. Rep. 3 (2013) 3009.
[25] D.P. Singh, A. George, R.V. Kumar, J.E. Elshof, M. Wagemaker, Nanostructured TiO_2 anatase micropatterned three-dimensional electrodes for high-performance Li-ion batteries, J. Phys. Chem. C 117 (2013) 19809.
[26] Y. Qu, W. Zhou, K. Pan, C. Tian, Z. Ren, Y. Dong, H. Fu, Hierarchical anatase TiO_2 porous nanopillars with high crystallinity and controlled length: an effective candidate for dye-sensitized solar-cells, PCCP 12 (2010) 9205.
[27] D.A. Richmond, Q. Zhang, G. Cao, D.N. Weiss, Pressureless nanoimprinting of anatase TiO_2 precursor films, J. Vac. Sci. Technol. B 29 (2011) 0216031.
[28] H. Segawa, H. Misawa, Fabrication of two-dimensional periodic TiO_2 pillar arrays by multi-beam laser interference lithography, Nat. Sci. 1 (2009) 176.
[29] E. Thimsen, N. Rastgar, P. Biswas, Nanostructured TiO_2 films with controlled morphology synthesized in a single step process: performance of dye-sensitized solar cells and photo watersplitting, J. Phys. Chem. C 112 (2008) 4134.
[30] A. Kumar, A.R. Madaria, C. Zhou, Growth of aligned single-crystalline rutile TiO_2 nanowires on arbitrary substrates and their application in dye-sensitized solar Cells, J. Phys. Chem. C 114 (2010) 7787.
[31] Y. Zhang, Y. Gao, X.H. Xia, Q.R. Deng, M.L. Guo, L. Wan, G. Shao, Structural engineering of thin films of vertically aligned TiO_2 nanorods, Mater. Lett. 64 (2010) 1614.
[32] C. Zhen, G. Liu, H.M. Cheng, A film of rutile TiO_2 pillars with well-developed facets on an a-Ti substrate as a photoelectrode for improved water splitting, Nanoscale 4 (2012) 3871.
[33] F. Cesano, D. Scarano, S. Bertarione, F. Bonino, A. Damin, S. Bordiga, C. Prestipino, C. Lamberti, A. Zecchina, Synthesis of ZnO-carbon composites and imprinted carbon by the pyrolysis of $ZnCl_2$-catalyzed furfuryl alcohol polymers, J. Photochem. Photobiol. A Chem. 196 (2008) 143.
[34] J.Y. Kim, J.H. Noh, K. Zhu, A.F. Halverson, N.R. Neale, S. Park, K.S. Hong, A.J. Frank, General strategy for fabricating transparent TiO_2 nanotube arrays for dye- sensitized photoelectrodes: illumination geometry and transport properties, ACS Nano 5 (2011) 2647.
[35] F. Cesano, S. Bertarione, A. Damin, G. Agostini, S. Usseglio, J.G. Vitillo, C. Lamberti, G. Spoto, D. Scarano, A. Zecchina, Oriented TiO_2 nanostructured pillar arrays: synthesis and characterization, Adv. Mater. 20 (2008) 3342.
[36] S. Cravanzola, G. Haznedar, D. Scarano, A. Zecchina, F. Cesano, Carbon-based piezoresistive polymer composites: structure and electrical properties, Carbon 62 (2013) 270.
[37] F. Cesano, I. Rattalino, F. Bardelli, A. Sanginario, A. Gianturco, A. Veca, C. Viazzi, P. Castelli, D. Scarano, A. Zecchina, Structure and properties of metal-free conductive tracks on polyethylene/multiwalled carbon nanotube composites as obtained by laser stimulated percolation, Carbon 61 (2013) 63.
[38] D. Scarano, S. Bertarione, F. Cesano, G. Spoto, A. Zecchina, Imaging polycrystalline and smoke MgO surfaces with atomic force microscopy: a case study of high resolu- tion image on a polycrystalline oxide, Surf. Sci. 570 (2004) 155.
[39] F. Cesano, M.M. Rahman, S. Bertarione, J.G. Vitillo, D. Scarano, A. Zecchina, Prepara- tion and adsorption properties of activated porous carbons obtained using volatile zinc templating phases, Carbon 50 (2012) 2047.
[40] M.M. Rahman, F. Cesano, F. Bardelli, D. Scarano, A. Zecchina, Hybrid SnO_2/carbon composites: from foams to films by playing with the reaction conditions, Catal. Today 150 (2010) 84.
[41] D.O. Scanlon, C.W. Dunnill, J. Buckeridge, S.A. Shevlin, A.J. Logsdail, S.M. Woodley, C.R.A. Catlow, M.J. Powell, R.G. Palgrave, I.P. Parkin, G.W. Watson, T.W. Keal, P. Sherwood, A. Walsh, A.A. Sokol, Band alignment of rutile and anatase TiO_2, Nat. Mater. 12 (2013) 798.
[42] M.-G. Ju, G. Sun, J. Wang, Q. Meng, W. Liang, Origin of high photocatalytic properties in the mixed-phase TiO_2: a first-principles theoretical study, ACS Appl. Mater. Interfaces 6 (2014) 12885.
[43] P. Yan, X. Wang, X. Zheng, R. Li, J. Han, J. Shi, A. Li, Y. Gan, C. Li, Photovoltaic device based on TiO_2 rutile/anatase phase junctions fabricated in coaxial nanorod arrays, Nano Energy 15 (2015) 406.